



Observation of the decay $B^0 \rightarrow D^\pm D^{*\mp}$

K. Abe⁴², R. Abe²⁹, T. Abe⁴³, H. Aihara⁴⁴, M. Akatsu²², Y. Asano⁴⁸, V. Aulchenko¹, T. Aushev¹², A. M. Bakich³⁹, Y. Ban³³, E. Banas²⁷, A. Bay¹⁸, I. Bedny¹, P. K. Behera⁴⁹, A. Bondar¹, A. Bozek²⁷, J. Brodzicka²⁷, T. E. Browder⁷, P. Chang²⁶, Y. Chao²⁶, B. G. Cheon³⁸, R. Chistov¹², S.-K. Choi⁶, Y. Choi³⁸, M. Danilov¹², L. Y. Dong¹⁰, A. Drutskoy¹², S. Eidelman¹, V. Eiges¹², Y. Enari²², H. Fujii⁸, C. Fukunaga⁴⁶, N. Gabyshev⁸, A. Garmash^{1,8}, T. Gershon⁸, B. Golob^{19,13}, A. Gordon²¹, R. Guo²⁴, F. Handa⁴³, T. Hara³¹, H. Hayashii²³, M. Hazumi⁸, E. M. Heenan²¹, T. Higuchi⁴⁴, L. Hinz¹⁸, T. Hojo³¹, T. Hokuue²², Y. Hoshi⁴², S. R. Hou²⁶, W.-S. Hou²⁶, H.-C. Huang²⁶, T. Igaki²², T. Iijima²², A. Ishikawa²², R. Itoh⁸, M. Iwamoto², H. Iwasaki⁸, Y. Iwasaki⁸, R. Kagan¹², J. Kaneko⁴⁵, J. H. Kang⁵², J. S. Kang¹⁵, P. Kapusta²⁷, N. Katayama⁸, H. Kawai², Y. Kawakami²², T. Kawasaki²⁹, H. Kichimi⁸, D. W. Kim³⁸, Heejong Kim⁵², H. J. Kim⁵², H. O. Kim³⁸, Hyunwoo Kim¹⁵, S. K. Kim³⁷, T. H. Kim⁵², K. Kinoshita⁴, S. Korpar^{20,13}, P. Krokovny¹, R. Kulasiri⁴, A. Kuzmin¹, Y.-J. Kwon⁵², J. S. Lange^{5,35}, S. H. Lee³⁷, J. Li³⁶, D. Liventsev¹², J. MacNaughton¹¹, G. Majumder⁴⁰, S. Matsumoto³, T. Matsumoto⁴⁶, K. Miyabayashi²³, H. Miyake³¹, H. Miyata²⁹, G. R. Moloney²¹, T. Mori³, T. Nagamine⁴³, Y. Nagasaka⁹, T. Nakadaira⁴⁴, E. Nakano³⁰, M. Nakao⁸, J. W. Nam³⁸, Z. Natkaniec²⁷, K. Neichi⁴², S. Nishida¹⁶, O. Nitoh⁴⁷, T. Nozaki⁸, S. Ogawa⁴¹, F. Ohno⁴⁵, T. Ohshima²², S. Okuno¹⁴, W. Ostrowicz²⁷, H. Ozaki⁸, P. Pakhlov¹², C. W. Park¹⁵, H. Park¹⁷, L. S. Peak³⁹, J.-P. Perroud¹⁸, L. E. Piilonen⁵⁰, F. J. Ronga¹⁸, N. Root¹, K. Rybicki²⁷, H. Sagawa⁸, S. Saitoh⁸, Y. Sakai⁸, M. Satapathy⁴⁹, A. Satpathy^{8,4}, O. Schneider¹⁸, S. Schrenk⁴, C. Schwanda^{8,11}, S. Semenov¹², K. Senyo²², M. E. Sevior²¹, H. Shibuya⁴¹, V. Sidorov¹, J. B. Singh³², S. Stanič^{48,*}, M. Starič¹³, A. Sugi²², A. Sugiyama²², K. Sumisawa⁸, T. Sumiyoshi⁴⁶, S. Suzuki⁵¹, S. Y. Suzuki⁸, S. K. Swain⁷, F. Takasaki⁸, K. Tamai⁸, N. Tamura²⁹, J. Tanaka⁴⁴, M. Tanaka⁸, G. N. Taylor²¹, Y. Teramoto³⁰, S. Tokuda²², T. Tomura⁴⁴, S. N. Tovey²¹, K. Trabelsi⁷, T. Tsuboyama⁸, T. Tsukamoto⁸, S. Uehara⁸, K. Ueno²⁶, Y. Unno², S. Uno⁸, Y. Ushiroda⁸, S. E. Vahsen³⁴, G. Varner⁷, K. E. Varvell³⁹, C. C. Wang²⁶, C. H. Wang²⁵, Y. Watanabe⁴⁵, E. Won¹⁵, B. D. Yabsley⁵⁰, Y. Yamada⁸, A. Yamaguchi⁴³, Y. Yamashita²⁸, M. Yamauchi⁸, H. Yanai²⁹, J. Yashima⁸, M. Yokoyama⁴⁴, Y. Yuan¹⁰, Y. Yusa⁴³, J. Zhang⁴⁸, Z. P. Zhang³⁶, V. Zhilich¹, and D. Žontar⁴⁸

(Belle Collaboration)

¹*Budker Institute of Nuclear Physics, Novosibirsk*

²*Chiba University, Chiba*

³*Chuo University, Tokyo*

⁴*University of Cincinnati, Cincinnati OH*

⁵*University of Frankfurt, Frankfurt*

⁶*Gyeongsang National University, Chinju*

⁷*University of Hawaii, Honolulu HI*

⁸*High Energy Accelerator Research Organization (KEK), Tsukuba*

⁹*Hiroshima Institute of Technology, Hiroshima*

¹⁰*Institute of High Energy Physics,
Chinese Academy of Sciences, Beijing*

¹¹*Institute of High Energy Physics, Vienna*

¹²*Institute for Theoretical and Experimental Physics, Moscow*

¹³*J. Stefan Institute, Ljubljana*

¹⁴*Kanagawa University, Yokohama*

¹⁵*Korea University, Seoul*

¹⁶*Kyoto University, Kyoto*

¹⁷*Kyungpook National University, Taegu*

¹⁸*Institut de Physique des Hautes Énergies,
Université de Lausanne, Lausanne*

¹⁹*University of Ljubljana, Ljubljana*

²⁰*University of Maribor, Maribor*

²¹*University of Melbourne, Victoria*

²²*Nagoya University, Nagoya*

²³*Nara Women's University, Nara*

²⁴*National Kaohsiung Normal University, Kaohsiung*

²⁵*National Lien-Ho Institute of Technology, Miao Li*

²⁶*National Taiwan University, Taipei*

²⁷*H. Niewodniczanski Institute of Nuclear Physics, Krakow*

²⁸*Nihon Dental College, Niigata*

²⁹*Niigata University, Niigata*

³⁰*Osaka City University, Osaka*

³¹*Osaka University, Osaka*

³²*Panjab University, Chandigarh*

³³*Peking University, Beijing*

³⁴*Princeton University, Princeton NJ*

³⁵*RIKEN BNL Research Center,
Brookhaven NY*

³⁶*University of Science and Technology of China, Hefei*

³⁷*Seoul National University, Seoul*

³⁸*Sungkyunkwan University, Suwon*

³⁹*University of Sydney, Sydney NSW*

⁴⁰*Tata Institute of Fundamental Research, Bombay*

⁴¹*Toho University, Funabashi*

⁴²*Tohoku Gakuin University, Tagajo*

⁴³*Tohoku University, Sendai*

⁴⁴*University of Tokyo, Tokyo*

⁴⁵*Tokyo Institute of Technology, Tokyo*

⁴⁶*Tokyo Metropolitan University, Tokyo*

⁴⁷*Tokyo University of Agriculture and Technology, Tokyo*

⁴⁸*University of Tsukuba, Tsukuba*

⁴⁹*Utkal University, Bhubaneswer*

⁵⁰*Virginia Polytechnic Institute and State University,
Blacksburg VA*

⁵¹*Yokkaichi University, Yokkaichi*

⁵²*Yonsei University, Seoul*

**on leave from Nova Gorica Polytechnic, Slovenia*

Abstract

We report the first observation of the decay $B^0 \rightarrow D^\pm D^{*\mp}$ with the Belle detector at the KEKB e^+e^- collider operated at the $\Upsilon(4S)$ resonance. Our analysis employs two methods of B^0 meson reconstruction: the full reconstruction method where both charmed mesons from B^0 decays are reconstructed and the partial reconstruction technique where only the slow pion from the $D^{*-} \rightarrow \bar{D}^0\pi^-$ decay and a fully reconstructed D^+ are used to reconstruct the B^0 . Using these two methods the sum of branching fractions $\mathcal{B}(B^0 \rightarrow D^+ D^{*-}) + \mathcal{B}(B^0 \rightarrow D^- D^{*+})$ is measured to be $(1.17 \pm 0.26^{+0.22}_{-0.25}) \times 10^{-3}$ and $(1.48 \pm 0.38^{+0.28}_{-0.31}) \times 10^{-3}$, respectively.

PACS numbers: 13.65.+i, 13.25.Gv, 14.40.Gx

Mixing-induced CP -violating asymmetries have been recently observed by the B factory experiments using modes with charmonia in the final state such as $B^0 \rightarrow J/\psi K_S^0$ [1]. With little theoretical ambiguity, the observed asymmetries determine $\sin 2\phi_1$, where ϕ_1 is one of the angles of the unitary triangle of the Cabibbo-Kobayashi-Maskawa matrix in the framework of the Standard Model. Further understanding of CP -violation and probes of new physics require measurements of CP -violation in additional decay modes. One class of such modes, the doubly-charmed decays $B^0 \rightarrow D^{(*)}D^{(*)}$, has attracted a great deal of attention [2]. While measurements of asymmetries in these modes are sensitive to $\sin 2\phi_1$, a deviation from the expected value is possible due to penguin contributions with additional phases from new physics. Among the doubly-charmed decays, $B^0 \rightarrow D^\pm D^{*\mp}$ is the most promising because neither an isospin analysis nor an angular analysis is necessary to measure ϕ_1 [3]. So far only an upper limit for the branching fraction of $B^0 \rightarrow D^\pm D^{*\mp}$ of 6.3×10^{-4} was obtained by the CLEO collaboration [4], although a naïve expectation for this branching fraction is 1.0×10^{-3} , scaling from the well measured branching fractions for the Cabibbo-allowed processes $B^0 \rightarrow D_s^+ D^{*-}$ and $B^0 \rightarrow D^- D_s^{*+}$ [5].

The data used for this analysis were taken with the Belle detector [6] at the KEKB asymmetric e^+e^- (3.5 on 8.0 GeV) collider [7]. The integrated luminosity used for this analysis is 29.4 fb^{-1} collected at the $\Upsilon(4S)$ resonance ($\sqrt{s} = 10.58 \text{ GeV}$) (referred to as on-resonance data) and 3.0 fb^{-1} at a center-of-mass (CM) energy just below the threshold of $B\bar{B}$ pair production (referred to as continuum data). The on-resonance data correspond to 31.9 million $B\bar{B}$ pairs. The Belle detector is a large-solid-angle magnetic spectrometer that consists of a three-layer silicon vertex detector (SVD), a 50-layer central drift chamber (CDC), a mosaic of aerogel threshold Čerenkov counters (ACC), time-of-flight scintillation counters (TOF), and an array of CsI(Tl) crystals (ECL) located inside a superconducting solenoid coil that provides a 1.5 T magnetic field. An iron flux-return located outside of the coil is instrumented to detect K_L mesons and to identify muons (KLM).

In the full reconstruction method we consider the decay $B^0 \rightarrow D^+ D^{*-}$ [8] followed by $D^{*-} \rightarrow \bar{D}^0 \pi^-$. Five decay modes are used for \bar{D}^0 reconstruction: $K^+ \pi^-$, $K^+ \pi^- \pi^- \pi^+$, $K_S^0 \pi^+ \pi^-$, $K^+ \pi^- \pi^0$ and $K^+ K^-$; D^+ mesons are reconstructed through $K^- \pi^+ \pi^+$ and $K_S^0 \pi^+$ decay modes.

Charged tracks are required to be consistent with the hypothesis that they originated from the interaction point in the r - ϕ plane. Charged kaon candidates are required to be positively identified. Only charged pion candidates involved in D^+ reconstruction are required to be positively identified to suppress the feed-down from the Cabibbo-allowed $B^0 \rightarrow D_s^{(*)+} D^{*-}$ decays.

K_S^0 candidates are reconstructed by combining $\pi^+ \pi^-$ pairs and requiring an invariant mass within $\pm 7.2 \text{ MeV}/c^2$ ($\pm 3\sigma$) of the nominal K_S^0 mass and that the pions are consistent with having originated from the same vertex. π^0 meson candidates are reconstructed from pairs of photons, each with energy greater than 0.1 GeV, that have an invariant mass within $\pm 13.5 \text{ MeV}/c^2$ ($\pm 3\sigma$) of the nominal π^0 mass. The \bar{D}^0 and D^+ candidates are required to have invariant mass within $\pm 2\sigma$ of the nominal masses, where σ is the channel-dependent mass resolution. D^{*-} candidates are formed from a \bar{D}^0 and a slow pion candidate (π_{slow}^-). We require the mass difference between D^{*-} and \bar{D}^0 to be within $\pm 11\sigma$ ($\sim 5 \text{ MeV}/c^2$) of the known mass difference to include large non-Gaussian D^{*-} tails in the $\bar{D}^0 \pi_{slow}^-$ mass distribution.

$B^0 \rightarrow D^+ D^{*-}$ candidates are selected using the CM energy difference, $\Delta E \equiv E_B - E_{beam}^{CM}$, and the beam-constrained mass $M_{bc} \equiv \sqrt{(E_{beam}^{CM})^2 - P_B^2}$, where $E_B(P_B)$ is the en-

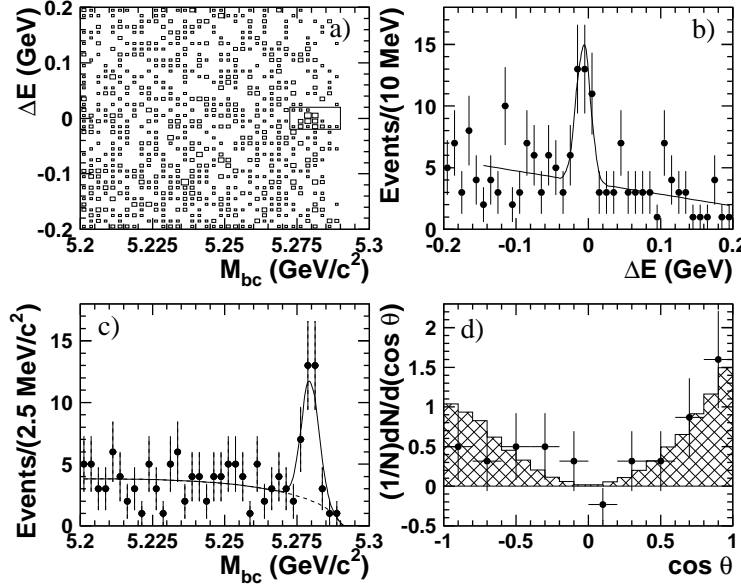


FIG. 1: Kinematical distributions of $B^0 \rightarrow D^+ D^{*-}$ candidates : a) scatter plot of ΔE versus M_{bc} ; b) ΔE projection for M_{bc} signal window, where the curve represents the fit described in the text; c) M_{bc} projection for ΔE signal window, where the curve represents the fit described in the text; d) $\cos \theta$ distributions for the data (points with error bars) and for the MC signal (shaded histogram).

ergy(momentum) of the B candidate and E_{beam}^{CM} is the CM beam energy. The scatter plot of ΔE versus M_{bc} , and the projections onto ΔE and M_{bc} are shown in Fig. 1a,b and c, respectively. If more than one candidate is found in an event, we use one of several criteria (e.g. best vertex-constrained fit of the D meson, number of CDC hits, best K_S^0 or π^0 fit), depending on the kind of ambiguity, to make a selection. For example, the best vertex-constrained fit is used to select among multiple D meson candidates. We define the signal region by $|\Delta E| < 0.02$ GeV and $5.225 < M_{bc} < 5.2900$ GeV/ c^2 , corresponding to $\sim \pm 2\sigma$ and $\sim \pm 2.5\sigma$ respectively. Forty candidates are found in the signal box. Fig. 1d shows the background subtracted helicity angle (θ) distribution of the D^{*-} candidate. The distribution follows the $\cos^2 \theta$ distribution that is expected for a pseudoscalar to pseudoscalar vector decay.

The signal resolution in M_{bc} is dominated by the beam energy spread, while the ΔE resolution is dominated by the energy resolutions of D^+ and D^{*-} . Therefore the M_{bc} distribution is less channel dependent and is more suitable for the extraction of the signal yield. We fit the M_{bc} projection with a Gaussian and the ARGUS background function [9]. The result is 29.6 ± 6.6 signal events. The statistical significance, defined as $\sqrt{-2 \ln(\mathcal{L}(0)/\mathcal{L}_{max})}$, is 7.0, where $\mathcal{L}_{max}(\mathcal{L}(0))$ is the maximized likelihood with(without) the signal contribution. A consistent yield (28.0 ± 7.0) is obtained by fitting the ΔE distribution with a Gaussian function over a linear background.

As possible sources which can contribute to the signal peak, we consider $B \rightarrow D^+ \pi_{slow}^- \bar{D}^0$ decay, where D^+ and π_{slow}^- come from resonant states ($D_1(2420)$ or $D_2(2460)$) or a non-resonant state. The resonant state contribution is checked using the invariant mass of the D^+ and π_{slow}^- . All the candidates have invariant mass below 2.2 GeV/ c^2 , hence there is no indication of resonant states of D^+ and π_{slow}^- . The non-resonant contribution is checked

TABLE I: The B reconstruction efficiencies (%) for the full reconstruction.

Channel	$K^+\pi^-$	$K^+\pi^-\pi^-\pi^+$	$K_S^0\pi^+\pi^-$	$K^+\pi^-\pi^0$	K^+K^-
$K^-\pi^+\pi^+$	10.7	3.81	3.88	2.60	7.78
$K_S^0\pi^+$	12.4	4.39	4.24	2.89	8.83

using the MC and found to be significantly suppressed by the D^{*-} selection requirements.

The reconstruction efficiencies for each of the ten subchannels are listed in Table I. For the branching fraction calculation the branching fraction $\mathcal{B}(\Upsilon(4S) \rightarrow B^0\bar{B}^0)$ is assumed to be 0.5. The systematic error is dominated by the uncertainty in the charged track reconstruction efficiency (2% for each track). The uncertainty in the signal yield is estimated by varying the signal and background parameters in the fit. Contributions to the systematic error are summarized in Table II. Finally, the branching fraction of $B^0 \rightarrow D^\pm D^{*\mp}$ is determined to be $(1.17 \pm 0.26^{+0.22}_{-0.25}) \times 10^{-3}$, where the first error is statistical and the second is systematic.

We also use the D^{*-} partial reconstruction technique previously used by the ARGUS and CLEO collaborations [10, 11, 12] which benefits from a higher B^0 reconstruction efficiency. B mesons produced in $\Upsilon(4S)$ decays have low CM momenta (≈ 340 MeV/c) resulting in charmed mesons from $B^0 \rightarrow D^+D^{*-}$ being almost back-to-back in the CM frame. The direction of the π_{slow}^- from the D^{*-} decay well approximates the direction of the mother particle due to the small energy release in the D^{*-} decay. Thus the CM angle α between π_{slow}^- and D^+ can be employed as a signature of this decay. Another signature of the decay $B^0 \rightarrow D^+D^{*-}$ is the D^{*-} polarization angle (θ) which can be calculated in the partial reconstruction technique using kinematical constraints. We use the CLEO definition of the polarization angle in a partial reconstruction [12]:

$$\cos \theta = \frac{-\beta_{D^*}(E_\pi^* - E_D^*)}{2P_\pi^*} + \frac{P_\pi^2 - P_D^2}{2\beta_{D^*}\gamma_{D^*}^2 M_{D^*} P_\pi^*},$$

where P_π (P_π^*) is the π_{slow}^- momentum in the CM frame (D^{*-} rest frame), and E_π^* (E_D^*) is the energy of the π_{slow}^- (D^0) in the D^{*-} rest frame. P_D , β_{D^*} and γ_{D^*} correspond to the \bar{D}^0 momentum in the CM frame and the Lorentz factors for D^{*-} , calculated using energy conservation and the known B^0 CM energy. The polarization angle distribution should exhibit a $\cos^2 \theta$ behavior due to the zero helicity state of the D^{*-} .

To suppress the backgrounds, which are much larger than for the full reconstruction method, tighter D^+ meson selection criteria are applied. D^+ mesons are reconstructed using the $K^-\pi^+\pi^+$ decay mode only. Tracks from D^+ meson decays are required to have associated SVD hits to guarantee a valid vertex reconstruction and are refitted to a common vertex. The good quality of the vertex fit is required. We exploit the relatively large D^+ decay length and require the decay path direction to be consistent with the momentum direction of the D^+ : $\cos(\vec{V}_D, \vec{P}_D)_{r-\phi} > 0$, where \vec{V}_D is a vector from the interaction point to the reconstructed D^+ vertex. This requirement has an efficiency of 87% for real D^+ s and suppresses the combinatorial background by a factor of two. The D^+ CM momentum is required to lie in the interval $1.63 < P_{D^+} < 1.97$ GeV/c and the π_{slow}^- is required to have CM momentum smaller than 0.2 GeV/c; these requirements are the kinematic limits for the studied decays.

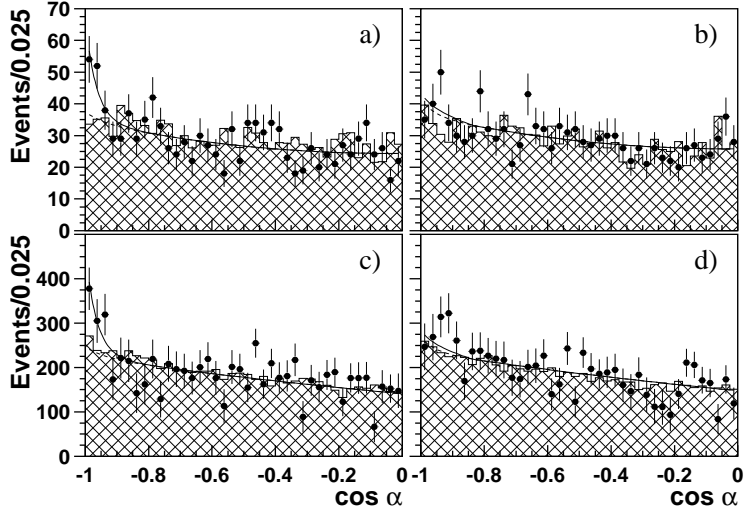


FIG. 2: a) and b) $\cos \alpha$ distributions for the leptonic sample, in regions *A* and *B* respectively; c) and d) $\cos \alpha$ distributions after continuum subtraction in the non-leptonic sample. Shaded histograms show the expected background distributions for generic $B\bar{B}$ MC. The curves represent the fit described in the text.

Some of the large backgrounds exhibit a similar angular tendency to the signal, *e.g.* the $c\bar{c}$ continuum background. Continuum events are partially removed by requiring the ratio of the second and zeroth Fox-Wolfram moments [13] to be smaller than 0.4. To disentangle the signal and the continuum background, the whole data sample is divided into two subsamples: the sample with a high-momentum lepton in the event (referred to below as “leptonic”), and the sample without high-momentum leptons (“non-leptonic” sample). Lepton candidates are required to be positively identified as either a muon or an electron and to have CM momenta larger than $1.1 \text{ GeV}/c$.

In the leptonic data sample, the presence of a high-momentum lepton in the event significantly reduces the continuum background. This background can be further suppressed using the angular correlation between the lepton and the D^+ candidate in the continuum. We require this angle to satisfy $-0.8 < \cos(\vec{P}_{D^+}, \vec{P}_{\ell^\pm}) < 0.9$. The continuum contribution is estimated to be smaller than 1% from the analysis of both continuum data and Monte Carlo simulation. In addition, this requirement removes a significant part of the $B\bar{B}$ background where the lepton and the D^+ originate from the same B meson.

The selected $D^+ \pi_{slow}^-$ combinations are divided into two independent regions of the polarization angle. The region $0.5 < |\cos \theta| < 1.05$ (referred to below as region *A*) contains 85% of the signal events, while the region $|\cos \theta| < 0.5$ (region *B*) is dominated by background. The distributions of $\cos \alpha$ for regions *A* and *B* are shown in Fig. 2*a,b*. The points with error bars are the data while the generic $B\bar{B}$ MC background distributions are superimposed and shown as shaded histograms. The $B^0 \rightarrow D_s^{(*)+} D^{*-}$ and $B^0 \rightarrow D^{*+} D^{*-}$ decay channels are excluded from the generic MC and are studied separately.

In the non-leptonic sample, the continuum data distributions of $\cos \alpha$ are scaled by a factor to account for the difference in the relative luminosities and cross-sections between on-resonance and continuum data and are then subtracted from the on-resonance data. The resulting $\cos \alpha$ distributions for regions *A* and *B* are shown in Fig. 2*c,d*. The data are the points with error bars while the generic $B\bar{B}$ MC background distributions are superimposed

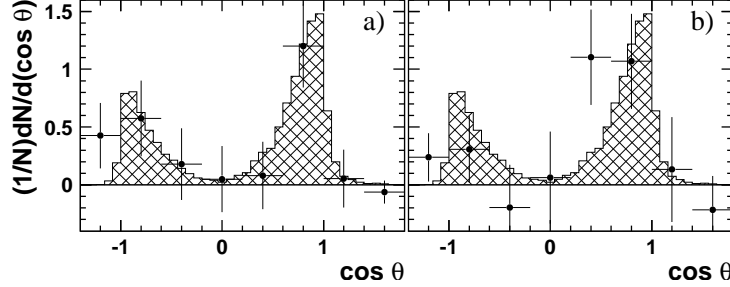


FIG. 3: Distributions of $\cos \theta$: a) leptonic sample; b) non-leptonic sample. Shaded histograms show the signal MC.

and shown as shaded histograms.

The contamination from $B^0 \rightarrow D_s^{(*)+} D^{*-}$ and $B^0 \rightarrow D^{*+} D^{*-}$, which produce similar peaks in the $\cos \alpha$ distribution are studied using the MC and normalized to the branching fractions measured in [4, 11]. We assume the D^{*-} is not polarized in these channels; the effect of possible D^{*-} polarization is included in the systematic error. The contributions of $B^0 \rightarrow D_s^{(*)+} D^{*-}$ in region A are estimated to be 4.0 ± 0.7 and 27 ± 5 events for leptonic and non-leptonic samples respectively; the $B^0 \rightarrow D^{*+} D^{*-}$ contributions are 3.0 ± 1.2 and 20 ± 8 events. Several other correlated backgrounds are studied in detail. The Cabibbo-allowed decays $B \rightarrow D^{*-} D^{(*)+} K$ result in D^+ CM momentum below our requirement and are completely rejected by the selection; for $B \rightarrow D_1(2420)(D_2^*(2460)) D^{(*)}$ decays the D^+ CM momentum is also shifted to lower values and these modes are strongly suppressed. The decays $B \rightarrow D^{(*)-} \rho$ and $B \rightarrow D^{(*)-} a_1$ are studied with different polarization hypotheses and are found not to produce a peak at $\cos \alpha = -1$. The possible contribution of these background sources is included in the systematic error.

Finally, each pair of $\cos \alpha$ distributions, Fig. 2(a,b) and (c,d), is fitted simultaneously to signal and background functions. The signal is parameterized by an exponential function which is a good description of the MC signal. The ratio of signal events in regions A and B is fixed according to the MC. The $B^0 \rightarrow D_s^{(*)+} D^{*-}$ and $B^0 \rightarrow D^{*+} D^{*-}$ background contributions are fixed in each region separately. The shape of other combinatorial backgrounds is parameterized by a second order polynomial that is assumed to be the same for regions A and B , in agreement with the MC. The fit finds 37.6 ± 13.2 and 283 ± 103 signal events in the leptonic and non-leptonic samples, respectively. As a cross-check, we fit the $\cos \alpha$ distribution in eight bins of $\cos \theta$. The resulting polarization angle distributions are shown in Fig. 3a and b for the leptonic and non-leptonic samples, respectively; the expected $\cos^2 \theta$ behavior can be seen in both samples.

One of the largest contributions to the systematic error in the signal yield is the uncertainty of the background shape. We use different background parameterizations to check the stability of the result against the choice of the background function. We also perform a fit with the background shape fixed from the generic $B\bar{B}$ MC. A summary of the systematic error sources is given in Table II.

The overall efficiencies estimated for the leptonic and non-leptonic samples are equal to 8.4×10^{-4} and 5.7×10^{-3} , respectively. We calculate the sum of branching fractions $\mathcal{B}(B^0 \rightarrow D^+ D^{*-}) + \mathcal{B}(B^0 \rightarrow D^- D^{*+})$ from the measurements with leptonic and non-leptonic samples to be $(1.41 \pm 0.52^{+0.27}_{-0.30}) \times 10^{-3}$ and $(1.57 \pm 0.57^{+0.30}_{-0.33}) \times 10^{-3}$, respectively, where the first error is statistical and the second is systematic. Averaging these two measurements we

TABLE II: Systematic errors on the branching fraction (%).

Error source	Full	Partial
Reconstruction efficiency	± 17	± 12
Particle identification	± 6	± 4
Signal and background shape	$^{+1}_{-7}$	$^{+13}_{-15}$
Correlated background	-	$^{+2}_{-3}$
Number of $B\bar{B}$ pairs	± 1	± 1
D branching fractions	± 7	± 7
Total	$^{+19}_{-21}$	$^{+19}_{-21}$

calculate $\mathcal{B}(B^0 \rightarrow D^+ D^{*-}) + \mathcal{B}(B^0 \rightarrow D^- D^{*+}) = (1.48 \pm 0.38^{+0.28}_{-0.31}) \times 10^{-3}$.

In summary, we report a measurement of the sum of the branching fractions for the decays $B^0 \rightarrow D^+ D^{*-}$ and $B^0 \rightarrow D^- D^{*+}$ using two analysis methods. The sum of the branching fractions $\mathcal{B}(B^0 \rightarrow D^+ D^{*-}) + \mathcal{B}(B^0 \rightarrow D^- D^{*+})$ is calculated to be $(1.17 \pm 0.26^{+0.22}_{-0.25}) \times 10^{-3}$ using the full reconstruction method and $(1.48 \pm 0.38^{+0.28}_{-0.31}) \times 10^{-3}$ using the partial reconstruction technique. These two measurements are not independent and should not be averaged. For calculations of the average branching fraction in this channel, the result from full reconstruction should be used. The partial reconstruction result is a consistency check and the sample obtained using this method will be used to improve statistics in future measurements of CP -violation. Our results are higher than the upper limit from CLEO; they are however consistent with the expectation based on $B^0 \rightarrow D^* D_s^{(*)}$.

We wish to thank the KEKB accelerator group for the excellent operation of the KEKB accelerator. We acknowledge support from the Ministry of Education, Culture, Sports, Science, and Technology of Japan and the Japan Society for the Promotion of Science; the Australian Research Council and the Australian Department of Industry, Science and Resources; the National Science Foundation of China under contract No. 10175071; the Department of Science and Technology of India; the BK21 program of the Ministry of Education of Korea and the CHEP SRC program of the Korea Science and Engineering Foundation; the Polish State Committee for Scientific Research under contract No. 2P03B 17017; the Ministry of Science and Technology of the Russian Federation; the Ministry of Education, Science and Sport of the Republic of Slovenia; the National Science Council and the Ministry of Education of Taiwan; and the U.S. Department of Energy.

[1] Belle Collaboration, K. Abe *et al.*, Phys. Rev. Lett. **87**, 091802 (2001); BaBar Collaboration, B. Aubert *et al.*, Phys. Rev. Lett. **87**, 091801 (2001).

[2] I. Dunietz *et al.*, Phys. Rev. D**43**, 2193 (1991); M. Ciuchini *et al.*, Phys. Rev. Lett. **79**, 978 (1997); A. I. Sanda and Z.-Z. Xing, Phys. Rev. D**56**, 341 (1997); X.-Y. Pham and Z.-Z. Xing, Phys. Lett. B**458**, 375 (1999).

[3] Z.-Z. Xing, Phys. Lett. B**443**, 365 (1998).

[4] CLEO Collaboration, E. Lipeles *et al.*, Phys. Rev. D**62**, 032005 (2000).

[5] D. E. Groom *et al.* (Particle Data Group), Eur. Phys. J. C**15**, 1 (2000).

- [6] Belle Collaboration, A. Abashian *et al.*, Nucl. Instr. and Meth. A**479**, 117-232 (2002).
- [7] KEKB B Factory Design Report, KEK Report 95-1, 1995, unpublished.
- [8] The charge conjugate modes are implicitly included.
- [9] ARGUS collaboration, H. Albrecht *et al.*, Phys. Lett. B**229**, 304 (1989); B**241**, 278 (1990).
- [10] ARGUS Collaboration, H. Albrecht *et al.*, Phys. Lett. B**324**, 249 (1994).
- [11] CLEO Collaboration, S. Ahmed *et al.*, Phys. Rev. D**62**, 112003 (2000).
- [12] CLEO Collaboration, G. Brandenburg *et al.*, Phys. Rev. Lett. **80**, 2762 (1998).
- [13] G. C. Fox and S. Wolfram, Phys. Rev. Lett. **41**, 1581 (1978).